ADVANCED FUNCTIONAL MATERIALS
www.afm-journal.de

Transparent, Anisotropic Biofilm with Aligned Bacterial Cellulose Nanofibers

*Sha Wang, Tian Li, Chaoji Chen, Weiqing Kong, Shuze Zhu, Jiaqi Dai, Alfredo J. Diaz, Emily Hitz, Santiago D. Solares, Teng Li, and Liangbing Hu**

Cellulose nanofibrils are attractive as building blocks for advanced photonic, optoelectronic, microfluidic, and bio-based devices ranging from transistors and solar cells to fluidic and biocompatible injectable devices. For the first time, an ultrastrong and ultratough cellulose film, which is composed of densely packed bacterial cellulose (BC) nanofibrils with hierarchical fibril alignments, is successfully demonstrated. The molecular level alignment stems from the intrinsic parallel orientation of crystalline cellulose molecules produced by Acetobacter xylinum. These aligned long-chain cellulose molecules form subfibrils with a diameter of 2–4 nm, which are further aligned to form nanofibril bundles. The BC film yields a record-high tensile strength (≈1.0 GPa) and toughness (≈25 MJ m^{-3}). Being ultrastrong and ultratough, yet the BC film is also highly flexible and can be folded into desirable shapes. The BC film exhibits a controllable manner of alignment and is highly transparent with modulated optical properties, paving the way to enabling new functionalities in mechanical, electrical, fluidic, photonics, and biocompatible applications.

1. Introduction

Cellulose is the most abundant organic material on earth, and has been ubiquitously used in daily life for thousands of years as information media. Recently, the utilization of strong and transparent cellulose films has found new advanced functionalities in emerging applications. With their unique microstructures, cellulose fibrils exhibit promising potential as alternative eco-friendly substrates for electronics, photonic, and energy storage devices.[1] Cellulose is also a highly biocompatible material, which can serve as an ideal scaffold for wearable or even injectable devices.[2] The inherent abundant hydroxyl groups on the surface of cellulose nanofibrils enable its utilization in a wide range of bio-based devices and functional nanomaterials,[1b,e,3] and as a biodegradable template for the synthesis of biomaterials with tailored functionality.[4] However, the cellulose nanofibrils (CNF) are often randomly distributed in the final products, which greatly limits their mechanical strength and restricts its realistic range of application.

CNF are made of aligned cellulose molecular chains at the molecular scale, achieving high strength ranging from 1.6 to 3.0 GPa for a single cellulose fibril.[5] However, alignment at a larger scale (fiber level) still presents great challenges. The current techniques for making CNF films typically result in fibrils with random orientation,[6] which limits their mechanical properties. For typical nanostructured materials including metal nanowires, graphene, carbon nanotube, and polycrystalline nanoscale units, it has been well-demonstrated that alignment (ordered structure) is important for achieving better mechanical properties.[7] Consequently, in order to explore the full potential of cellulose fibril and to obtain exceptional mechanical properties to enable new functionalities in optoelectronic, microfluidic, and biocompatible devices, it is highly desirable to obtain a controllable manner to accomplish high quality fibril alignment in a scalable process. However, alignment on the microscale still presents great challenges and has been rarely achieved in CNFs. CNFs have been mainly manufactured from plants, in which the other components such as lignin and hemicellulose need to be removed by chemical treatment beforehand.[8] Chemical, enzymatic, or mechanical pretreatments need to be applied for CNF purification.[9] During those processes, the natural fibril alignment and the integration of crystalline cellulose chains are unavoidably lost with largely weakened mechanical properties.[10] To fully explore the possible applications including optoelectronics, fluidic, and biodevices, it is highly desirable to obtain controllable alignment of high-quality intact cellulose chains while maintaining the original properties of cellulose fibrils.

In this work, we use quantitative stretching to control the degree of alignment of bacterial cellulose (BC) fibrils. We have successfully produced transparent biofilms with hierarchical structural alignment. Our aligned BC film exhibits a record high strength, surpassing that of all-cellulose based paper,

S. Wang, Dr. T. Li, Dr. C. Chen, W. Kong, J. Dai, E. Hitz, Prof. L. Hu
Department of Materials Science and Engineering
University of Maryland College Park
College Park, MD 20742, USA
E-mail: binghu@umd.edu
Dr. S. Zhu, Prof. T. Li
Department of Mechanical Engineering
University of Maryland College Park
College Park, MD 20742, USA
A. J. Diaz, Prof. S. D. Solares
Department of Mechanical and Aerospace Engineering
The George Washington University
Washington, DC 20052, USA
The ORCID identification number(s) for the author(s) of this article can be found under https://doi.org/10.1002/adfm.201707491.

DOI: 10.1002/adfm.201707491

and even other types of randomly oriented or aligned fibrils including organic cross-linked polymers.[11] The ultrastrong and ultratough BC film is also of high flexibility and can be folded into complex shapes, a highly desirable but often hard to achieve combination of superb mechanical properties. Moreover, our BC film has tunable optical properties owing to its intact molecular level alignment and increased crystallization, proven superior over the typical cellulose-based transparent papers derived from plants. We demonstrate that the aligned BC film can yield anisotropic optical properties, which can be tailored by tuning the wet-drawing strain level. The unique tunable anisotropic optical functionality along with its ultrahigh strength and toughness yet high flexibility positions our BC biofilm as a promising candidate for future applications in structural materials, flexible electronics, and photonics.

2. Results and Discussion

As shown in **Figure 1**, acetobacter xylium extrudes BC nanofibrils with high crystallinity that are naturally aligned at the molecular scale. The cellulose chains tend to orient themselves in the planar direction of the film and form aligned subfibrils. The cellulose nanofibrils are composed of an aligned bundle of subfibrils. The original BC nanofibrils in a wet membrane are randomly distributed. By applying a direct drawing, an alignment ranging from nanoscale to microscale can be achieved in the same direction as the molecular alignment direction. The atomic force microscope (AFM) images clearly indicate that the BC nanofibrils in the BC network become highly oriented along the stretching direction. With maximized alignment area between long and intact nanofibrils, the toughness and strength of the BC film are greatly increased simultaneously, a highly desirable feature given that these two mechanical properties are often mutually exclusive (e.g., the stronger, the less tougher).[11,12] Consequently, we demonstrated that our BC film can be made into an origami plane (Figure 1).

In a typical experiment, as-grown BC pellicles (Figure S1a,b, Supporting Information) were purified and then cut into a rectangular shape of size 20 mm × 70 mm (Figure S1c, Supporting Information). Then BC films with different wet-drawing strains were obtained by a novel developed fully stretching method. Herein, the wet-drawing strain is defined as the percentage ratio between the stretching-induced length increase value and the length of the original wet BC film (Figure S2, Supporting Information). It is found that the maximum wet-drawing strain that could be achieved without failure of the structural integrity is around 20% (Figure S3, Supporting Information). The failure of cellulose network structure after strain at 20% can be ascribed to the damage of tightly entangled nanofibrils resulting from the tension force during wet-drawing process. To overcome the disadvantage of alignment by only stretching using tensile machine, we developed a novel step to improve the alignment degree. After stretching to 20% wet-drawing strain, the stretched BC films were repeatedly shaken to loosen the entangled cellulose nanofibrils and homogenize the alignment in the transverse direction and then stretched again, thus increasing the alignment of the resulting products. Hence, BC films with 30% and 40% wet-drawing strain were prepared. To confirm the effectiveness of the developed methods, the surface morphologies of BC nanocellulose films with different wet-drawing strain were observed by field emission scanning electron microscope (FE-SEM) (**Figure 2**a–d). The original BC film contains randomly distributed nanofibrils with a diameter of around 30 nm (Figure 2a), which is the typical size of bundled elementary fibrils.[12b] The 20% wet-stretched BC film (Figure 2b) shows an increasing amount of aligned BC nanofibrils. After further increasing the wet-drawing strain to 30% (Figure 2c), more

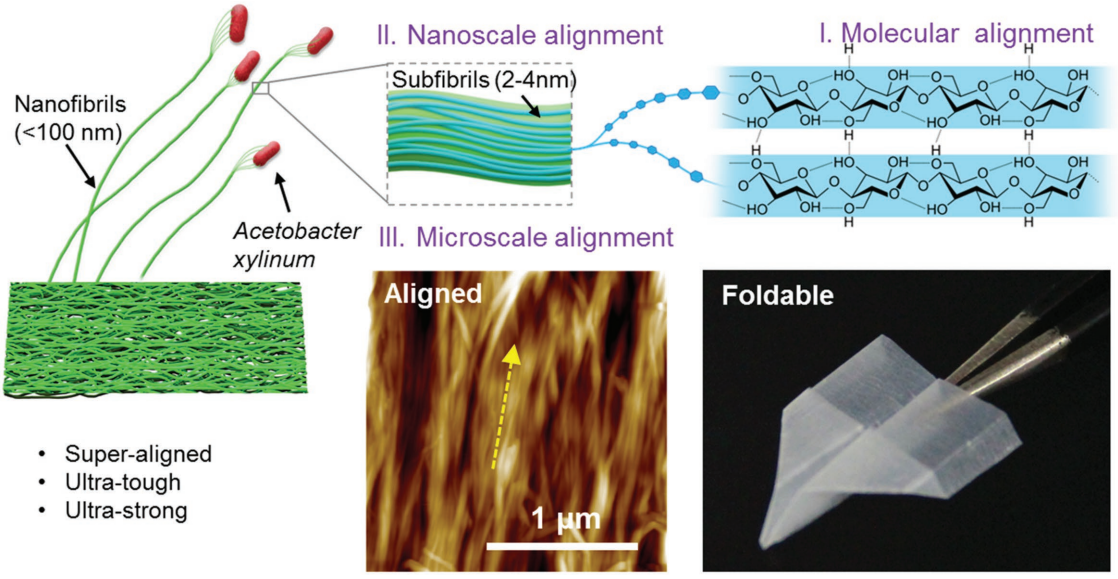

Figure 1. Schematic of the formation of an ultrastrong and ultratough cellulose film. Acetobacter xylinum produces cellulose chains with high crystallinity that are aligned on the molecular level, which are further aligned to form subfibrils with a diameter of 2–4 nm. The BC fibril bundles have a diameter of 20–100 nm in the original film and result from a self-assembling of subfibrils. The film morphology and multiscale alignment is well preserved which results in an ultrastrong, ultratough, and flexible cellulose film. Thus, our BC film can be folded into an origami plane.

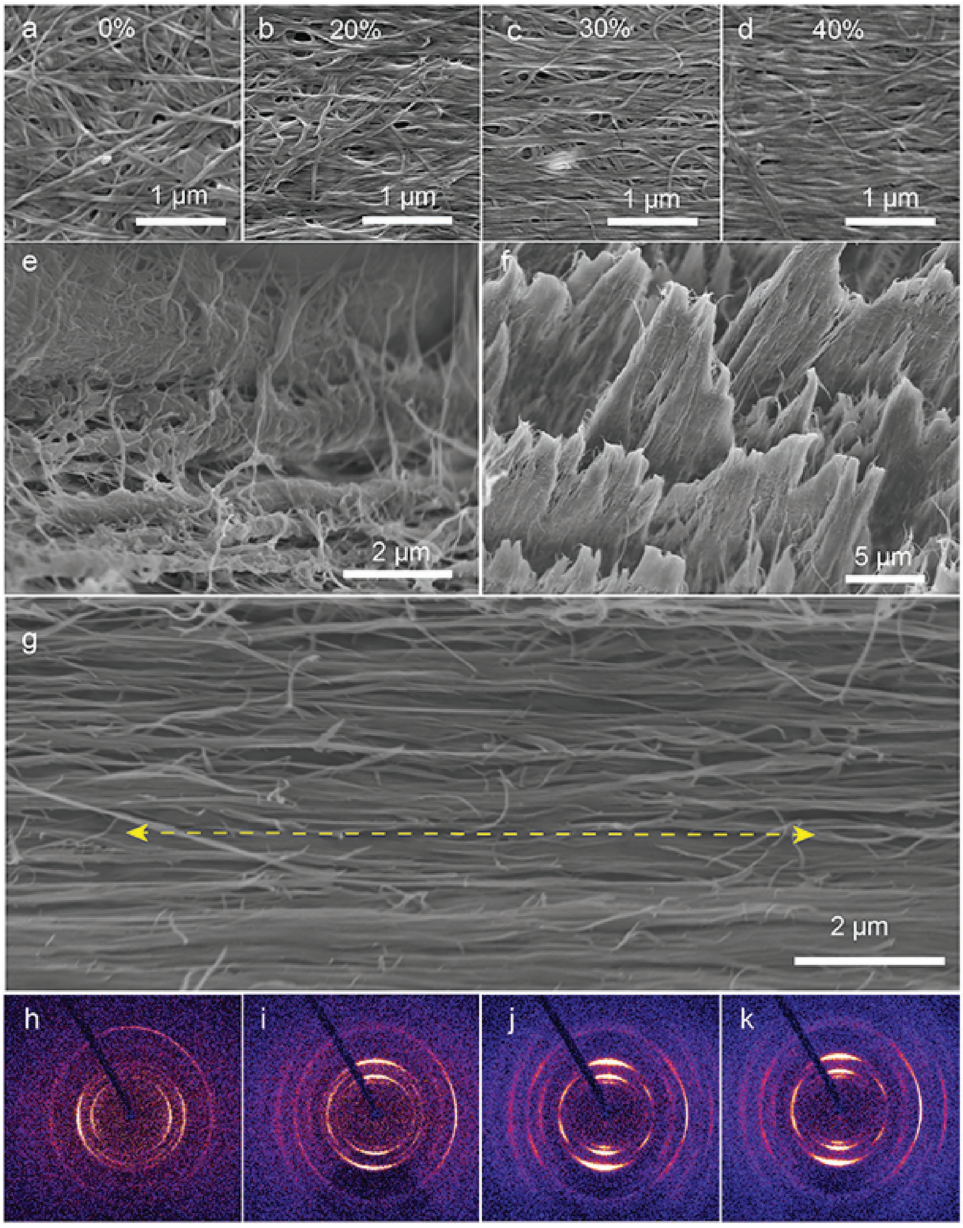

Figure 2. Images and diffractograms of nonstretched and stretched BC films. a–d) SEM images of the surface of 0%, 20%, 30%, and 40% wet-drawn BC films. e,f) Cross-sectional images of nonstretched and 40% wet-drawn BC films perpendicular to the stretching direction. Cellulose microfibril bundles are observed in the 40% BC film, resulting from the strong hydrogen bonding between highly aligned nanofibrils formed during the wet-drawing process. g) Side view of 40% wet-drawn BC film parallel to the stretching direction. h–k) WAXS diffractograms of 0%, 20%, 30%, and 40% strain wet-drawn BC films. The vertical arcs become brighter with higher wet-drawing strain level, indicating an increasing alignment of the cellulose nanofibrils.

aligned nanofibrils are observed while the original network structure can be barely recognized. When the BC pellicle is wet-stretched under 40% strain, a few wrinkles appear that are parallel to each other, showing a well aligned structure at the microscale (Figure S4, Supporting Information).

At high magnification, SEM imaging clearly shows that individual BC nanofibrils become densely packed and are aligned parallel to each other, leading to the complete disappearance of the original random network structure (Figure 2d). The morphology of the resulting BC film was also characterized by AFM (Figure S5, Supporting Information), which confirms the fibril alignment observed in FE-SEM images. The cross-section morphologies of the nonstretched and stretched films are investigated by FE-SEM (Figure 2e,f). A layered structure is apparent in the original BC film (Figure 2e). After 40% stretching, cellulose starts to appear in the form of fibril bundles (Figure 2f), indicating the formation of strong hydrogen bonding between the highly aligned nanofibrils during the wet-stretching process. The side view of 40% wet-drawn sample along the stretching direction clearly shows the well-aligned nanofibrils structure (Figure 2g), confirming the successful improvement using our developed method.

Inside the aligned fiber bundles, the nanoscale alignment after drying has been well preserved, as indicated by the wide-angle X-ray scattering (WAXS) results (Figure 2h–k), in which the incoming X-ray beam is perpendicular to the surface of BC films. The diffractogram of the original BC film shows three intense arcs on the equator, suggesting that a low degree of orientation exists in the original BC film (Figure 2h), which may be caused by shrinkage during drying.[8a] At higher strain, the arcs near the vertical polar axis become brighter (Figure 2i–k), indicating an increasing amount of alignment of the cellulose nanofibrils. In addition, a macroscopic alignment of BC nanofibrils is confirmed by the gradual deformation of the small angle X-ray scattering (SAXS) 2D patterns (from 0% to 40% strain) (Figure S6, Supporting Information).

The tensile strength and toughness of our BC films that undergo different stretching levels are tested (**Figure 3**a, **Table 1**). The morphologies of the fracture surface of nonstretched and 40% wet-drawn BC films are shown in Figure 3b,c. A loose and porous structure is presented in the cross-sectional image of the original BC film with a small number of cellulose nanofibers pulled out from the broken film (Figure 3b). Such loose and porous fracture surface suggests a weak hydrogen bonding between the randomly

Table 1. Mechanical properties of as-prepared BC films under different wet-drawing strains.

Wet-drawing strain [%]	Strain at break [%]	Young's modulus [GPa]	Tensile strength [MPa]	Toughness [MJ m^{-3}]
0	3.4	11.4	194.4	3.8
20	3.4	40.4	327.4	6.6
30	4.2	40.5	684.5	16.2
40	4.4	48.1	1005.3	24.7

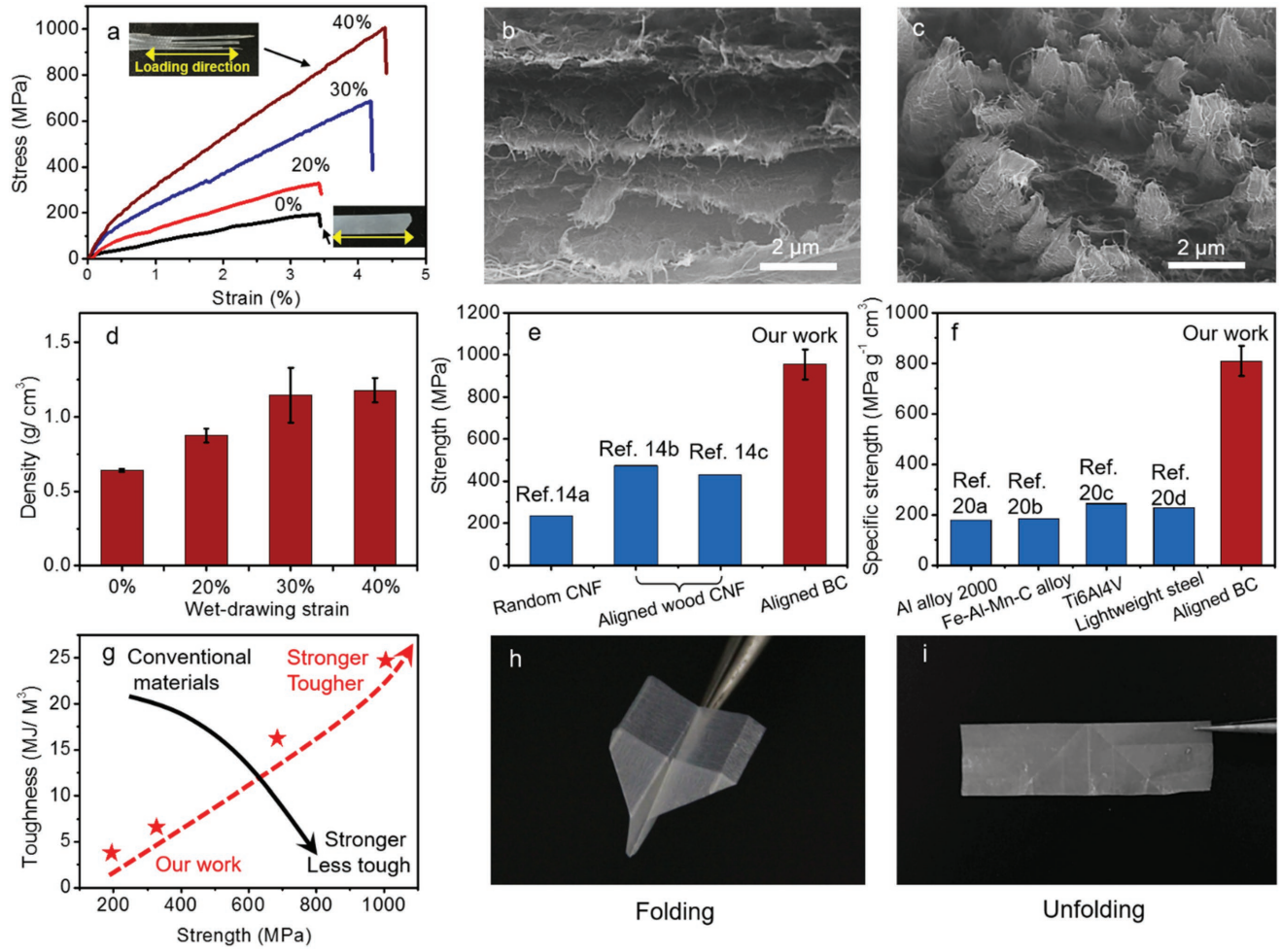

Figure 3. Superb mechanical properties of BC films: ultrastrong and tough yet highly foldable. a) Stress–strain curves of BC films before and after stretching. The inset photographs show the morphology of the original and 40% wet-drawing BC films at break. b,c) Cross-sectional images of fracture surfaces of as-grown and 40% wet-drawn BC film, respectively. d) A density plot of BC film under different wet–drawing strains. e) Comparison of tensile strength of pure cellulose-based papers. A record-high strength up to 1.0 GPa was obtained for our 40% stretched BC film. f) Specific tensile strength of aligned BC film compared with novel lightweight and strong metallic alloys. g) The scaling law of simultaneous increase in toughness and strength of our BC films, which sharply contrasts with conventional material behaviors. The result of this study is shown in red stars. h,i) A photograph shows a paper airplane made with 40% wet-drawing BC film (h), and the film after unfolding (i), as can be clearly observed, the folding line is almost invisible, indicating truly foldable properties. The error bars denote one standard deviation of the mean in (e,f).

oriented fibrils, resulting in a low mechanical tensile strength. In sharp contrast, as shown in the cross-sectional surface image of the 40% stretched BC film (Figure 3c), a much denser fracture surface with a large number of cellulose nanofibers pulled out from the broken film can be observed. The tensile stretching induces nanoscale alignment of the nanofibrils and forms densely packed microfibril bundles, indicating the strong interaction (mainly refers to hydrogen bonding here) among the cellulose nanofibers. This can be further confirmed by the optical microscope observation (Figure S7, Supporting Information).

The densities of BC film under 0%, 20%, 30%, and 40% wet-drawing strain are 0.64 g cm^{-3}, 0.88 g cm^{-3}, 1.14 g cm^{-3}, and 1.18 g cm^{-3}, respectively (Figure 3d), indicating an increasing fibril density upon stretching. Apparently, tensile strength, modulus, and toughness increase significantly with increasing wet-drawing strain. For the nonstretched BC film, the tensile strength is 194.4 MPa, which is consistent with the values reported in previously work.[12] The exceptional mechanical properties of the unstretched BC film are associated with highly crystalline cellulose from bacterial biosynthesis. Interestingly, the mechanical properties of the BC film can be further enhanced with increasing structural alignment. When prestretched to 20% strain, the aligned BC film shows a significantly improved tensile strength (327.4 MPa) as well as toughness (6.6 MJ m^{-3}), which are 1.7 times, and 1.7 times those of the original one, respectively. Upon further increasing the wet-drawing strain, a decrease of stress is clearly observed in the wet BC pellicle, indicating the damage of cellulose nanofibrils in the wet BC network structure (Figure S3, Supporting Information). Further confirmed by a recent publication, aligned BC array with a maximum tensile strength of 260.4 MPa at 20% wet-drawing strain was produced by a combination of PDMS grating substrate-guided BC growth and wet-stretching methods.[13] However, using our well-developed design of shaking and further deforming after the initial machine stretching, a larger wet-drawing strain (40%) is obtained. The potential reason for this result is that entangled nanofibrils become loose during shaking, which can allow for further alignment through additional stretching, avoiding early fracture of the cellulose nanofibrils. Notably, for 40% stretched BC film, the tensile strength can be up to a record-high 1.005 GPa. To our best knowledge, this is the strongest of any all-cellulose films reported so far, rendering it a biocompatible ultrastrong cellulose substrate.

Interestingly, a higher wet-drawing strain level leads to an increase in strength and modulus along with improved toughness (Table 1). Under increasing wet-drawing strain from 0% to 40%, tensile strength increases from 194.4 MPa to 1.005 GPa, Young's modulus increases from 11.4 to 48.1 GPa, and toughness increases from 3.8 to 24.7 MJ m^{-3}. Our 40% BC film exhibits a maximum tensile strength, up to ≈1.0 GPa (Table 1), and the average value is 955 ± 71 MPa, a record-high strength compared with other all-cellulose based papers (Figure 3e; Table S1, Supporting Information).[14] The tensile strength for 40% wet-drawing BC film is even higher than those of previously reported studies including 40% drawing cellulose nanopapers from wood cellulose nanofibrils (428 ± 15 MPa),[14c] CNF filaments prepared by hydrodynamic alignment (490 ± 86 MPa),[15] CNF filaments prepared from wood cellulose nanofibrils (321 MPa),[16] bioplastics obtained from microcrystalline cellulose and edible vegetable waste (Figure S8, Supporting Information),[17] electrospun axially aligned cellulose fiber mats (Figure S9, Supporting Information),[18] and aligned BC films.[13,19]

Recently, macroscopic CNF ribbon was fabricated by aligning cellulose nanofibrils grafted with polyethylene glycol via stretching. However, time-consuming steps were required before achieving nanofibrils alignment by stretching.[11] Aligned BC arrays were produced by BC guided growth by gating substrate and additional stretching methods.[13,19b] A maximum tensile strength of 260.4 MPa under wet-stretching strain 20% was reported, which increased by 256% in comparison to original BC pellicles.[13] The above-mentioned stretching is typically achieved using a tensile testing machine, which typically leads to the early fracture of regional cellulose nanofibrils due to the inhomogeneous alignment along the transverse direction. Thus it gave rise to a low wet-stretching strain (20%), which reduces the degree of alignment of the cellulose nanofibrils and the mechanical properties of the resulting products. Furthermore, we also compare the specific tensile strength of the present study with selected metallic alloys of high specific strength (Figure 3f).[20] Interestingly, the specific tensile strength of our aligned BC is as high as 809 ± 60 MPa g^{-1} cm^3, which is even higher than that of newly developed low-density alloys. Our obtained value is 4.5 times, 4.4 times, 3.3 times, and 3.6 times that of aluminum alloy 2000 (179 MPa g^{-1} cm^3),[20a] Fe-Al-Mn-C alloy (183 MPa g^{-1} cm^3),[20b] titanium alloy (244 MPa g^{-1} cm^3),[20c] and lightweight high-specific-strength steel (227 MPa g^{-1} cm^3),[20d] respectively.

It is noteworthy that typical cellulose-based films exhibit an inverse correlation between strength and toughness (Figure 3g).[14b] In sharp contrast, our BC film exhibits an increasing strength along with an increasing toughness. This simultaneous rise in toughness and strength with increasing web-drawing strain can be understood as follows. On one hand, an increasing wet-drawing strain leads to a higher packing density of the resulting BC film. As a result, the defect size and density due to misalignment of BC nanofibrils decrease, which in turn lead to a significantly enhanced tensile strength. On the other hand, a BC film with a higher web-drawing strain has much more aligned BC nanofibrils as well as a higher packing density. Both features contribute to significantly increased interaction area between cellulose nanofibrils, allowing for facile re-formation of hydrogen bonding between neighboring cellulose nanofibrils during stretching and thus leading to a much increased toughness of the BC film.[21] Note that the anomalous but desirable scaling behavior of strength and toughness of BC films in this study results from increasing fibril alignment, different from a previous report in which such a scaling law in cellulose films originates from decreasing fibril diameter.[21] Although wood CNF papers typically exhibit good flexibility, a CNF paper with foldability is still a challenge. Here, we have demonstrated that our BC film is truly foldable and can be folded into an origami plane (Figure 3h). Upon unfolding, the BC film does not show visible degradation (Figure 3i), showing its tough and flexible properties.

Note that the stability of cellulose-based film against humidity or water is critical for some practical applications. In this context, we further carried out water uptake experiments.

We immersed those films into water, or put them in humidity chamber with humidity of 20% and 80%. After stabilization at each humidity condition, we then measured their water absorption capacity by calculating the mass of absorbed water per unit mass of dry films. Additionally, we have compared the water absorption capacities of those films with that of common paper. As shown in Figure S10 (Supporting Information), when put in water, all four BC films show lower water absorption than the normal printing paper. Comparing the four BC films, the sample with a higher wet-drawing stain exhibits a lower water absorption content, which we ascribe to the denser structure of the higher wet-drawing BC film. When the humidity becomes lower, the water absorption content significantly decreases to a relatively low value, similar to the recently reported work.[17] Our results show that the 40% BC film is much more stable than normal printing paper when exposed to water.

We have also carried out mechanical tensile tests for our BC biofilms after conditioning under a high relative humidity of 80%, and compared the results to our previous results obtained in a low relative humidity of 40%. As shown in Figure S11 (Supporting Information), at both humidity conditions, the tensile strength increased with increasing wet-drawn strain. When comparing the mechanical tensile strength obtained at different humidity levels, we can observe that higher relative humidity (80%) conditioning slightly decreases the tensile strengths of all four samples, which should be attributed to the increased water absorption in a higher humidity condition. Higher water content will weaken the connection (mainly refers to hydrogen bonding here) between the cellulose nanofibers, thus leading to a lower mechanical strength.

To qualitatively shed light on the underlying mechanism of the superb mechanical properties of the highly aligned BC film, we have performed molecular dynamics simulations on a scaled-down model, which contains well-aligned cellulose chains, randomly-dispersed cellulose chains, and aligned short chains (see Figure S12 in the Supporting Information for modeling details). The length of each constituent cellulose chain in the aligned-short model is about half of that of the aforementioned well-aligned model. This is to simulate the situation for cellulose fibrils extracted from plants. The cellulose nanofibrils become shorter than the original ones because of chemical treatment and high shear forces that take place during the pulping and defibrillation processes.[22] We have computed the averaged virial stress of each atom in the system for these three model systems. The stress–strain curves (**Figure 4**a) clearly show that the well-aligned model exhibits both strength and toughness that are exceptionally higher than those of the randomly aligned model. For example, the maximum stress in the well-aligned model (Figure 4a, red line) is 1.92 times that of the random model (Figure 4a, black line). The toughness (area underneath the stress–strain curve) in the well-aligned model is 10.3 times that of the random model. The simulation also shows that both the maximum stress and toughness in the aligned-short model decreases compared to that of the model with longer chains. For example, the maximum stress and toughness in the aligned model with longer chains (red line) are 1.84 times and 4.48 times those of the aligned model with shorter chains (purple line), respectively. This confirms that BC aligned fibril films can exhibit much better mechanical properties than paper made from cellulose extracted from plants. The decrease in the maximum stress as the chain length decreases can be understood as follows. In a well-aligned model, there is a maximized number of interfaces at which individual cellulose chains could slide over each other. We assume the initial contact length (assuming hydrogen-bonded) between two cellulose chains is L, the hydrogen bonding energy per length is λ, the hydrogen bonding interfacial shear strength per length is γ. Considering the breaking and reforming of hydrogen bonds, the energy dissipated to separate these two chains in a sliding mode is proportional to $\int_0^L \lambda \, dl$, and the maximum force during sliding is proportional to γL. For a well-aligned model with longer chains, L is typically larger, and therefore results in an increase in both strength and toughness.

A further investigation on the deformation trajectory (Figures S13 and S14, Supporting Information) reveals the structural contributions leading to such a significant difference in mechanical properties. The initial models of well-aligned, randomly dispersed, and aligned short cellulose chains are shown (Figure 4b–d, top view). On one hand, the well-aligned model (Figure 4e) could induce a maximized number of interfaces at which each individual cellulose chain could slide over each other, an advantage that the random and aligned-short (Figure 4f,g) models do not possess. The sliding is resisted by the need to break hydrogen bonds. With more of these interfaces, the structure as a whole can distribute higher mechanical load, leading to an enhanced strength. We have found in our simulations that under the same equilibrated pressure, the well-aligned structure has the smallest specific volume (thus the highest density, in agreement with experimental results), which further suggests a higher packing efficiency of these well-aligned cellulose chains that could maximize the number of inter-chain hydrogen bonding interfaces.

The anisotropic microstructure of the BC biofilm with multiscale alignment of high aspect ratio cellulose can lead to anisotropic optical properties. To validate this, we measure the optical properties of the four BC biofilms with various degrees of alignment. As can be clearly observed, the anisotropic structures in the BC film that underwent different amounts of strain (0%, 20%, 30%, and 40%) lead to tunable anisotropic optical properties (**Figure 5**). The light scattering setup (Figure S15, Supporting Information) shows that a single mode laser with an emission wavelength of 532 nm (Thorlabs, Inc.) was first collimated with an ≈200 μm spot size before perpendicular illumination of the samples. For the nonstretched BC film, the transmission pattern rapidly diverges in the x and y directions due to its isotropic scattering in the cross-sectional plane of light propagation. While the incoming light spot follows the standard Gaussian distribution, the full width at half maximum of the transmitted light spot remains the same in both the x and y directions. The scattering effect is isotropic in the light propagation cross-section plane for the nonstretched BC film (Figure 5a). On the other hand, 20%, 30%, and 40% stretched BC yield highly anisotropic optical transmission (Figure 5b–d) with rapidly diverging light intensity in the y direction (the BC fibrils are aligned along the x direction).

The light intensity distribution in both the x and y direction of the 2D plane perpendicular to the light propagation direction (z direction) was plotted respectively. The nanofibrils in the

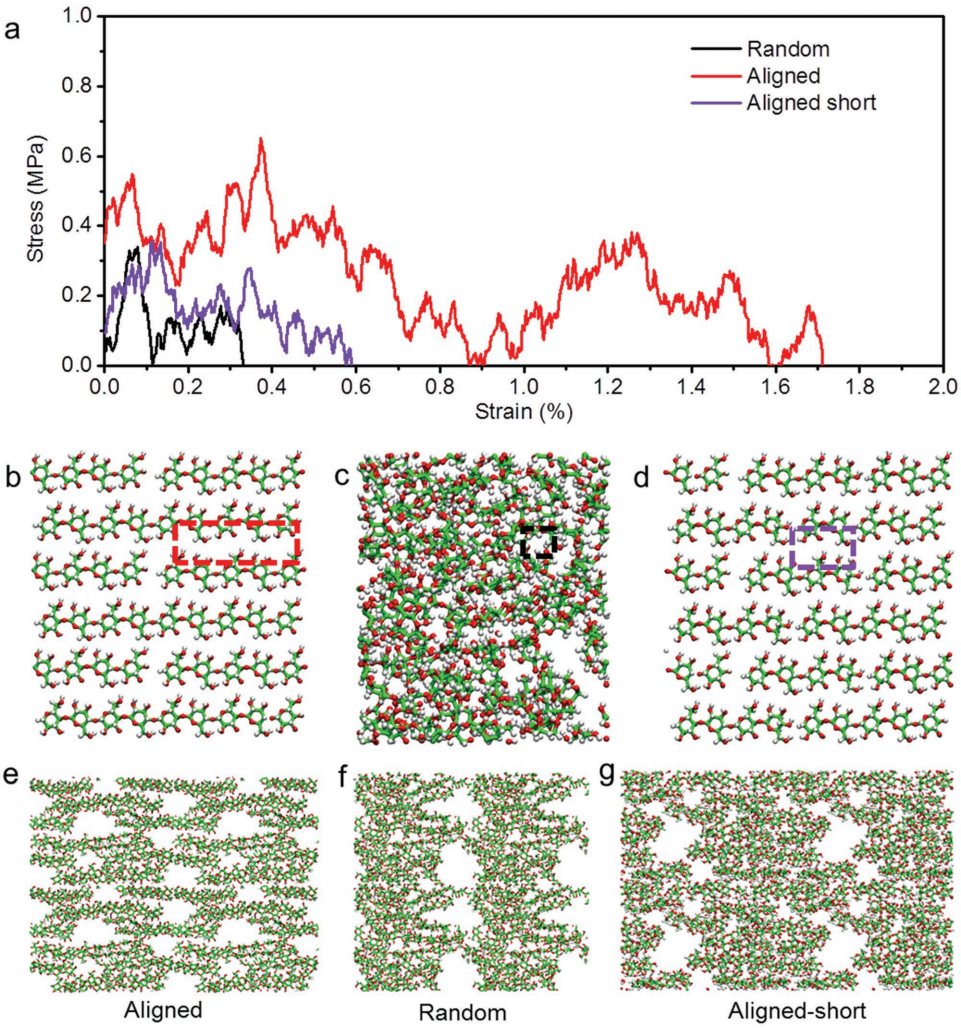

Figure 4. Molecular dynamic simulations on well-aligned, randomly-dispersed, and aligned short cellulose chains. a) Averaged virial stress per atom calculated from MD simulations as a function of the strain applied to the simulation box. The red, purple, and black lines correspond to well-aligned cellulose chains models, aligned cellulose short chains model, and random cellulose chains models, respectively. Red line corresponds to an aligned model whose cellulose chain length is about half of that of the other aligned model (purple line). b–d) Initial model on aligned (b), random (c), and aligned-short (d) cellulose chains. Dashed boxes show the corresponding hydrogen bonding areas. e) Deformation snapshots of the well-aligned model at a strain of 0.25. Four periodic images are patched together for visual assistance. The tensile strain is applied horizontally. f) Deformation snapshots of the randomly aligned model at a strain of 0.25. g) Deformation snapshots of the aligned short fibril model at a strain of 0.25.

nonstretched BC film are oriented randomly. The resulting scattered light thus exhibits a Gaussian-like distribution with a similar scattering angle in both the x and y directions. On the other hand, the stretched BC fibrils are highly aligned in the x direction, yielding a discrete index variation in the y direction. An increasingly traverse-expanded beam is observed in the y direction with a larger scattering angle upon higher stretching level (Figure 5b–d). This results from the strong light diffraction by densely packed and aligned BC fibrils. A general trend is observed that higher wet-drawing strain leads to a higher anisotropy (Figure 5e,f). Interestingly, different scattering patterns can be achieved by stacking two layers of wet-drawn BC films, exhibiting great promise in optical applications with tunable light transmission patterns (Figure 5g). In addition to the anisotropic behavior of optical properties, we also investigated the total transmittance and optical transmittance haze of the original and 40% wet-drawn BC samples using an integrated sphere and UV–vis Spectrometer Lambda 35 (PerkinElmer, USA). Both the original and stretched films show high transmittance (91% at 800 nm) covering the entire visible wavelength ranging from 400 to 800 nm (Figure 5h,i). The haze for 40% stretched sample is twice that of the original one (0%), indicating a large scattering effect across the fibril alignment direction. To directly observe the unique imaging effect of the BC film with controllable alignment, we have put a 0% BC film and a 40% BC film on top of a grid pattern (Figure S16, Supporting Information). When placed directly on top, the vertical and parallel lines can be clearly observed. When placed just 1 cm above, the grids become blurry for the 0% BC film. In comparison, the vertical lines shown through the 40% BC film are clearer than the parallel lines owning to the anisotropic scattering effect. Our developed BC film exhibits a controllable

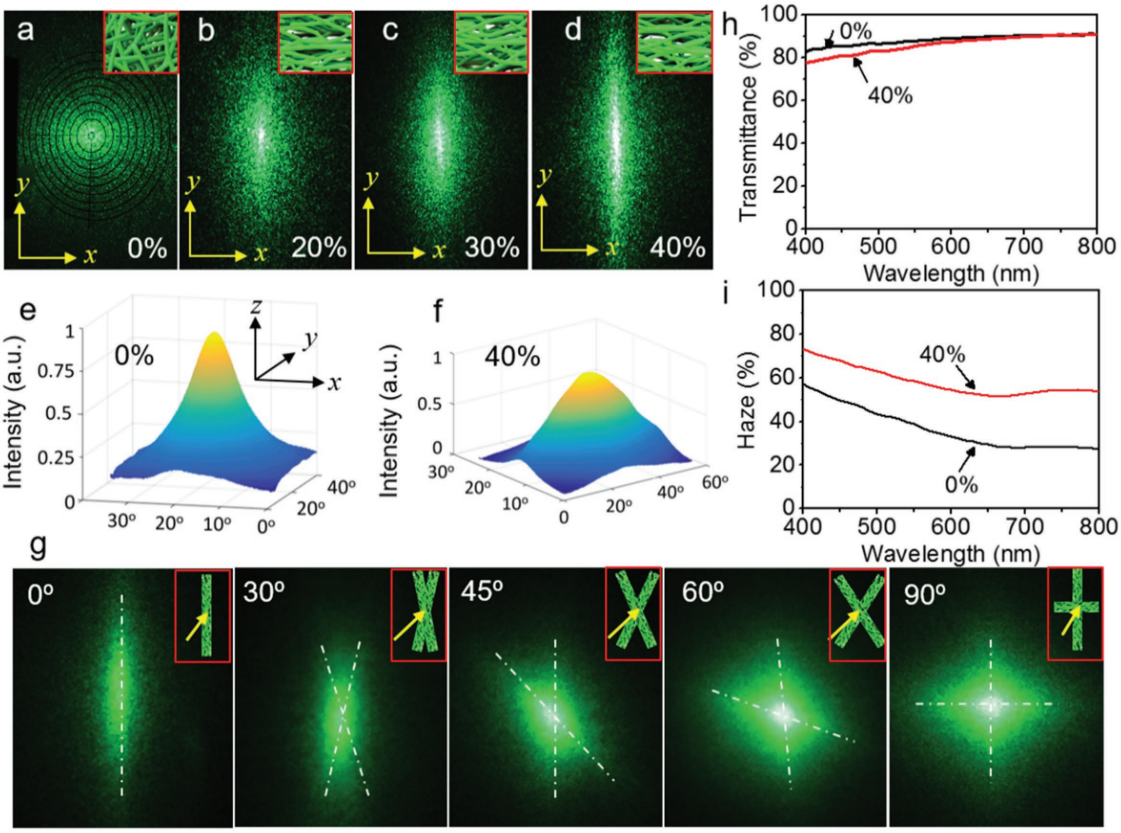

Figure 5. Characterization of tunable optical properties of BC films. a–d) Light scattering effect of BC films stretched to 0%, 20%, 30%, and 40% strain, respectively. The anisotropic light scattering effect is due to the formation of highly aligned BC fibrils structures. e,f) Angle-dependent scattering spectra intensity plots for 0% and 40% wet-drawing films. g) Light scattering effects of two pieces of 40% wet-stretched BC films stacked at different cross angles. The white dashed lines are drawn as a visual guide. h,i) Broadband transmittance and haze measurement of the original and stretched BC films.

manner of light management, which can function as a light diffuser with high optical transmittance where the distribution of light can be modulated. Large directional scattering was realized which can help cast an evenly distributed light along a desirable direction or following a desirable shape.

3. Conclusions

In conclusion, we report a transparent BC film via hierarchical alignment from molecular level crystalline cellulose chain alignment to microscale level fibrils bundle alignment. The intrinsic superb properties of the cellulose fibrils have been largely preserved and a high level of alignment is obtained. This contributes to a maximized interaction area of long chain cellulose fibrils and an efficient reformation of hydrogen bonding upon stretching, exhibiting a desirable scaling law of being simultaneously stronger and tougher. The resulting super-aligned BC film showed a record-high tensile strength, up to 1.0 GPa, and an ultrahigh toughness of 24.7 MJ m^{-3}, both of which are the highest among previously demonstrated all-cellulose based flexible paper, and thereby can find use in safety-critical applications where catastrophic device failure needs to be prevented. Our foldable BC film exhibits an extremely high specific tensile strength of 852 MPa g^{-1} cm^3, which is even stronger than titanium alloys. The aligned BC film also exhibits a broadband high transparency covering the entire visible range with the capability of wide range optical modulation. The ultrastrong and tough yet highly flexible and transparent BC films with added optical properties can find a range of potential applications in lightweight devices, structural materials, and optoelectronics.

4. Experimental Section

Materials Preparation: Bacterial cellulose was produced by the bacterial *Acetobacter xylinum* (strain ATCC 1765), which was inoculated into 15 mL of a Hestrin and Schramm (HS) medium in a beaker at 30 °C in a rotary shaker. The inoculum contained 20.0 g L^{-1} glucose, 5.0 g L^{-1} peptone, 5.0 g L^{-1} yeast extract, 2.7 g L^{-1} Na_2HPO_4, and 1.5 g L^{-1} citric acid. Before culturing, the medium was autoclaved at 121 °C for 15 min. A pellicle of bacterial cellulose was obtained after incubation in static state at 30 °C for 7 d. The as-prepared bacterial cellulose was soaked into 0.5 mol L^{-1} sodium hydroxide solution and then washed to a pH of 7.0 with a substantial amount of deionized water to eliminate residual dead cells and chemicals.

BC Films Fabrication: BC films were prepared by cutting a piece of purified BC pellicle into a rectangular shape of size 20 mm × 70 mm, then wet-drawn using a Tinius Olsen H25KT testing machine at a crosshead speed of 1 mm min^{-1} with a gauge length of 60 mm until the strain of the sample reached 20%. Subsequently, the 20% wet-drawn

samples were unloaded from the tensile testing machine, shaken repeatedly, and further stretched to achieve higher wet-drawing strain by loosening the entangled cellulose nanofibrils, and homogenizing degree of alignment in the transverse direction. Hence films with wet-drawn strain of 30% and 40% were obtained. The wet-drawn samples were placed in between layers of filter papers and hot pressed at 60 °C for 24 h using a Carver press machine. For comparison purposes, the original BC films (0%) were prepared in the same manner by processing from a piece of the same BC pellicle.

Measurements and Characterization: The morphology was examined at the surface of the original BC films and the wet-drawn BC films using AFM and FE-SEM. The FE-SEM experiment was conducted with a Hitachi SU-70 SEM working at an acceleration voltage (10 kV) and short working distance (7 mm). The cross-section samples were prepared by immersion in liquid nitrogen followed by fracture of nonstretched BC films.

An Asylum Research Cypher S microscope equipped with an ARC2 SPM controller operated in tapping mode was used for the AFM experimental measurements. The cantilever was an Olympus AC160TS probe with a natural frequency near 292.1 kHz, which was driven with a free oscillation amplitude of ≈43 nm and a 67% setpoint. The nominal force constant is 26 N m^{-1}. The samples were directly attached to magnetic stubs using adhesive tape and scanned in the microscope. Topographic (height) images were recorded.

Wide-angle X-ray diffraction data were collected on a Rigaku RAPID II equipped with a curved detector manufactured by Rigaku Americas Corp using CuKα radiation (λ = 0.1541 nm) at an operating tube voltage of 40 kV and tube current of 30 mA. 2D diffraction patterns were recorded by mounting BC samples perpendicular with respect to the incident beam. Data conversion and analysis were processed through Rigaku software packages 2DP (version 1.0.3.4) and PDXL 2 (version 2.0.3.0).

Tensile tests of the samples were performed using a Tinius Olsen H25KT testing machine. Specimens of ≈3 mm width were tested at a gauge length of 25 mm and a cross-head speed of 5 mm min^{-1}. All specimens were conditioned at a relative humidity of 40% for 48 h at 23 °C before testing. The Young's modulus was determined as the slope at low strain and the tensile strength was determined as the stress at specimen breakage. Toughness was defined as the work required to achieve fracture and was calculated as the area under the stress–strain curve.[23] The density of the BC film was determined by dividing the sample weight by the sample volume as measured by a digital caliper.

For SAXS experiments, a Xenocs Xeuss system having a 3D beam generator with Cu Kα X-ray radiation with a wavelength of 1.5418 Å (GeniX, Xenocs SA, France) was used. The 2D scattering data were collected with a 300 K Dectris Pliatus detector (pixel size of 172 µm × 172 µm). The sample-to-detector distance was 196.511 mm.

For water uptake measurements, the water content of all samples was initially calculated. All samples were weighed on a sensitive electronic balance and then weighed again after drying at 105 °C for 4 h. The water content of samples was defined as the mass change per the oven dried mass of the sample. Afterward, all BC films and printing paper were weighed and then conditioned in a 20% or 80% relative humidity chamber at room temperature. After 24 h in the chamber, all samples were weighed again. To measure the water absorption, the samples were weighed and then immersed in a large amount of water at room temperature for 30 min. Afterward, the samples were weighed again. The amount of water adsorption (absorption) was calculated based on the gained mass per over mass of the sample.

Light transmittance of the BC samples was measured using a visible spectrophotometer (CARY 50 Bio, Varian) with a wavelength range of 400 to 800 nm. A 532 nm single mode DJ532-10 laser (Thorlabs, Inc.) was used as the incoming light source with stabilized output power. The laser was collimated first with a spot size around 200 µm before perpendicularly illuminating the samples. The Gaussian beam quickly diverged after propagating through the transparent BC films.

Supporting Information

Supporting Information is available from the Wiley Online Library or from the author.

Acknowledgements

S.W., T.L., C.C., and W.K. contributed equally to this work. The authors acknowledge the Maryland NanoCenter and its NispLab. A.J.D. and S.D.S. acknowledge support from the US Department of Energy, Office of Science, Basic Energy Sciences, under Award No. DESC0011912.

Conflict of Interest

The authors declare no conflict of interest.

Keywords

anisotropic biofilms, bacterial cellulose, biofilms, multiscale alignment, transparent biofilms

Received: December 25, 2017
Published online: February 23, 2018

[1] a) H. Zhu, W. Luo, P. N. Ciesielski, Z. Fang, J. Zhu, G. Henriksson, M. E. Himmel, L. Hu, *Chem. Rev.* **2016**, *116*, 9305; b) R. J. Moon, A. Martini, J. Nairn, J. Simonsen, J. Youngblood, *Chem. Soc. Rev.* **2011**, *40*, 3941; c) L. Nyholm, G. Nyström, A. Mihranyan, M. Strømme, *Adv. Mater.* **2011**, *23*, 3751; d) Z. Wang, C. Xu, P. Tammela, J. Huo, M. Strømme, K. Edström, T. Gustafsson, L. Nyholm, *J. Mater. Chem. A* **2015**, *3*, 14109; e) Y. H. Jung, T.-H. Chang, H. Zhang, C. Yao, Q. Zheng, V. W. Yang, H. Mi, M. Kim, S. J. Cho, D.-W. Park, *Nat. Commun.* **2015**, *6*, 7170; f) E. Fortunato, D. Gaspar, P. Duarte, L. Pereira, H. Águas, A. Vicente, F. Dourado, M. Gama, R. Martins, in *Bacterial Nano-Cellulose: From Biotechnology to Bio-Economy* (Eds: M. Gama, F. Dourado, S. Bielecki), Elsevier, Oxford **2016**, pp. 179–196; g) S.-J. Chun, E.-S. Choi, E.-H. Lee, J. H. Kim, S.-Y. Lee, S.-Y. Lee, *J. Mater. Chem.* **2012**, *22*, 16618; h) J. Cai, J. Chen, Q. Zhang, M. Lei, J. He, A. Xiao, C. Ma, S. Li, H. Xiong, *Carbohydr. Polym.* **2016**, *140*, 238.

[2] Q. Niu, K. Gao, Z. Shao, *Nanoscale* **2014**, *6*, 4083.

[3] a) M. Rezayat, R. K. Blundell, J. E. Camp, D. A. Walsh, W. Thielemans, *ACS Sustainable Chem. Eng.* **2014**, *2*, 1241; b) J. Guo, I. Filpponen, P. Su, J. Laine, O. J. Rojas, *Cellulose* **2016**, *23*, 3065; c) Z. Shi, Y. Li, X. Chen, H. Han, G. Yang, *Nanoscale* **2014**, *6*, 970; d) S. Li, D. Huang, B. Zhang, X. Xu, M. Wang, G. Yang, Y. Shen, *Adv. Energy Mater.* **2014**, *4*, 1301655; e) Z. Shi, G. O. Phillips, G. Yang, *Nanoscale* **2013**, *5*, 3194; f) S. Rajala, T. Siponkoski, E. Sarlin, M. Mettänen, M. Vuoriluoto, A. Pammo, J. Juuti, O. J. Rojas, S. Franssila, S. Tuukkanen, *ACS Appl. Mater. Interfaces* **2016**, *8*, 15607; g) Q. Zheng, Z. Cai, Z. Ma, S. Gong, *ACS Appl. Mater. Interfaces* **2015**, *7*, 3263.

[4] a) J. T. Korhonen, P. Hiekkataipale, J. Malm, M. Karppinen, O. Ikkala, R. H. Ras, *ACS Nano* **2011**, *5*, 1967; b) M. S. Toivonen, A. Kaskela, O. J. Rojas, E. I. Kauppinen, O. Ikkala, *Adv. Funct. Mater.* **2015**, *25*, 6618.

[5] T. Saito, R. Kuramae, J. Wohlert, L. A. Berglund, A. Isogai, *Biomacromolecules* **2012**, *14*, 248.

[6] X. Xu, F. Liu, L. Jiang, J. Zhu, D. Haagenson, D. P. Wiesenborn, *ACS Appl. Mater. Interfaces* **2013**, *5*, 2999.

[7] a) L.-B. Mao, H.-L. Gao, H.-B. Yao, L. Liu, H. Cölfen, G. Liu, S.-M. Chen, S.-K. Li, Y.-X. Yan, Y.-Y. Liu, *Science* **2016**, *354*, 107; b) L. Sun, K. Keshoju, H. Xing, *Nanotechnology* **2008**, *19*, 405603; c) D. Jang, X. Li, H. Gao, J. R. Greer, *Nat. Nanotechnol.* **2012**, *7*, 594; d) G. Xin, T. Yao, H. Sun, S. M. Scott, D. Shao, G. Wang, J. Lian, *Science* **2015**, *349*, 1083; e) Z. Zhou, X. Wang, S. Faraji, P. D. Bradford, Q. Li, Y. Zhu, *Carbon* **2014**, *75*, 307.

[8] a) N. Lavoine, I. Desloges, A. Dufresne, J. Bras, *Carbohydr. Polym.* **2012**, *90*, 735; b) W. Wang, M. D. Mozuch, R. C. Sabo, P. Kersten, J. Zhu, Y. Jin, *Cellulose* **2015**, *22*, 351; c) M. Jonoobi, R. Oladi, Y. Davoudpour, K. Oksman, A. Dufresne, Y. Hamzeh, R. Davoodi, *Cellulose* **2015**, *22*, 935.

[9] a) M. Henriksson, G. Henriksson, L. Berglund, T. Lindström, *Eur. Polym. J.* **2007**, *43*, 3434; b) W. Chen, H. Yu, Y. Liu, Y. Hai, M. Zhang, P. Chen, *Cellulose* **2011**, *18*, 433; c) Y. Li, Y. Liu, W. Chen, Q. Wang, Y. Liu, J. Li, H. Yu, *Green Chem.* **2016**, *18*, 1010; d) I. A. Sacui, R. C. Nieuwendaal, D. J. Burnett, S. J. Stranick, M. Jorfi, C. Weder, E. J. Foster, R. T. Olsson, J. W. Gilman, *ACS Appl. Mater. Interfaces* **2014**, *6*, 6127.

[10] A. Isogai, T. Saito, H. Fukuzumi, *Nanoscale* **2011**, *3*, 71.

[11] H. Tang, N. Butchosa, Q. Zhou, *Adv. Mater.* **2015**, *27*, 2070.

[12] a) Y. Huang, C. Zhu, J. Yang, Y. Nie, C. Chen, D. Sun, *Cellulose* **2014**, *21*, 1; b) W. Gindl, J. Keckes, *Compos. Sci. Technol.* **2004**, *64*, 2407.

[13] M. M. Rahman, A. N. Netravali, *ACS Macro Lett.* **2016**, *5*, 1070.

[14] a) H. Fukuzumi, T. Saito, T. Iwata, Y. Kumamoto, A. Isogai, *Biomacromolecules* **2008**, *10*, 162; b) C. Baez, J. Considine, R. Rowlands, *Cellulose* **2014**, *21*, 347; c) H. Sehaqui, N. Ezekiel Mushi, S. Morimune, M. Salajkova, T. Nishino, L. A. Berglund, *ACS Appl. Mater. Interfaces* **2012**, *4*, 1043.

[15] K. M. Håkansson, A. B. Fall, F. Lundell, S. Yu, C. Krywka, S. V. Roth, G. Santoro, M. Kvick, L. P. Wittberg, L. Wågberg, *Nat. Commun.* **2014**, *5*, 4018.

[16] S. Iwamoto, A. Isogai, T. Iwata, *Biomacromolecules* **2011**, *12*, 831.

[17] I. S. Bayer, S. Guzman-Puyol, J. A. Heredia-Guerrero, L. Ceseracciu, F. Pignatelli, R. Ruffilli, R. Cingolani, A. Athanassiou, *Macromolecules* **2014**, *47*, 5135.

[18] a) X. He, Q. Xiao, C. Lu, Y. Wang, X. Zhang, J. Zhao, W. Zhang, X. Zhang, Y. Deng, *Biomacromolecules* **2014**, *15*, 618; b) H. Q. Liao, Y. Q. Wu, M. Y. Wu, X. R. Zhan, H. Q. Liu, *Cellulose* **2012**, *19*, 111.

[19] a) A. Nagashima, T. Tsuji, T. Kondo, *Carbohydr. Polym.* **2016**, *135*, 215; b) M. M. Rahman, A. N. Netravali, *Compos. Sci. Technol.* **2016**, *136*, 85.

[20] a) T. Dursun, C. Soutis, *Mater. Des.* **2014**, *56*, 862; b) Y. Sutou, N. Kamiya, R. Umino, I. Ohnuma, K. Ishida, *ISIJ Int.* **2010**, *50*, 893; c) F. Gil, J. Manero, M. Ginebra, J. Planell, *J. Mater. Sci. Eng. A* **2003**, *349*, 150; d) S.-H. Kim, H. Kim, N. J. Kim, *Nature* **2015**, *518*, 77.

[21] H. Zhu, S. Zhu, Z. Jia, S. Parvinian, Y. Li, O. Vaaland, L. Hu, T. Li, *Proc. Natl. Acad. Sci. USA* **2015**, *112*, 8971.

[22] a) S. Gharehkhani, E. Sadeghinezhad, S. N. Kazi, H. Yarmand, A. Badarudin, M. R. Safaei, M. N. M. Zubir, *Carbohydr. Polym.* **2015**, *115*, 785; b) R. Shinoda, T. Saito, Y. Okita, A. Isogai, *Biomacromolecules* **2012**, *13*, 842.

[23] M. Henriksson, L. A. Berglund, P. Isaksson, T. Lindstrom, T. Nishino, *Biomacromolecules* **2008**, *9*, 1579.

ADVANCED FUNCTIONAL MATERIALS

Supporting Information

for *Adv. Funct. Mater.*, DOI: 10.1002/adfm.201707491

Transparent, Anisotropic Biofilm with Aligned Bacterial Cellulose Nanofibers

*Sha Wang, Tian Li, Chaoji Chen, Weiqing Kong, Shuze Zhu, Jiaqi Dai, Alfredo J. Diaz, Emily Hitz, Santiago D. Solares, Teng Li, and Liangbing Hu**

Supporting Information

Transparent, Anisotropic Biofilm with Aligned Bacterial Cellulose Nanofibers

Sha Wang[1(a)], Tian Li[1(a)], Chaoji Chen[1(a)], Weiqing Kong[1(a)], Shuze Zhu[2], Jiaqi Dai[1], Alfredo J. Diaz[3], Emily Hitz[1], Santiago D. Solares[3], Teng Li[2], Liangbing Hu*[,1]

[1]Department of Materials Science and Engineering, University of Maryland College Park, College Park, Maryland, 20742

[2]Department of Mechanical Engineering, University of Maryland College Park, College Park, Maryland, 20742

[3]Department of Mechanical and Aerospace Engineering, The George Washington University, Washington, District of Columbia, 20052

[(a)] These authors contributed equally to this work.

* Correspondence: binghu@umd.edu

BC pellicle fabrication.

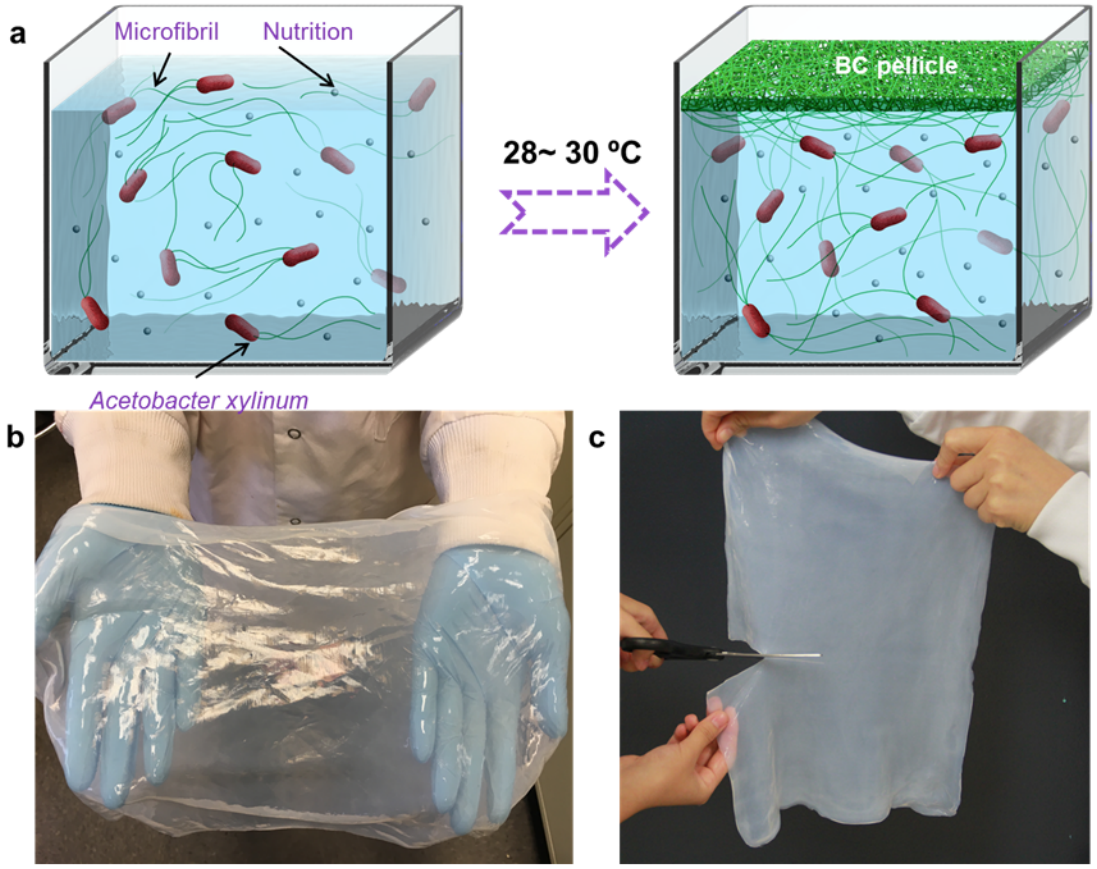

Figure S1. Through a fermentation process (a) a large piece of purified BC pellicle (b) with 99.4% of water content can be large-scale generated, which greatly reduces the cost for the production of transparent and ultra-strong film. BC transparent films are prepared by cutting a piece of purified BC pellicle into a rectangular shape of size 20 mm × 70 mm (c), then wet-drawn until the strain of the sample reached 20%, 30%, and 40%, respectively.

Stretching test setup

A schematic of the stretching process is shown in Figure S2 (a). The wet-drawing strain is defined as the percentage of length difference before and after drawing divided by the initial length of the BC pellicle. Figure S2 (b) shows a strip of BC pellicle (20 mm×70 mm) mounted between two grips. The bottom grip is fixed on the base and the top grip can be displaced up and down. After stretching, a wide BC strip becomes narrower and longer.

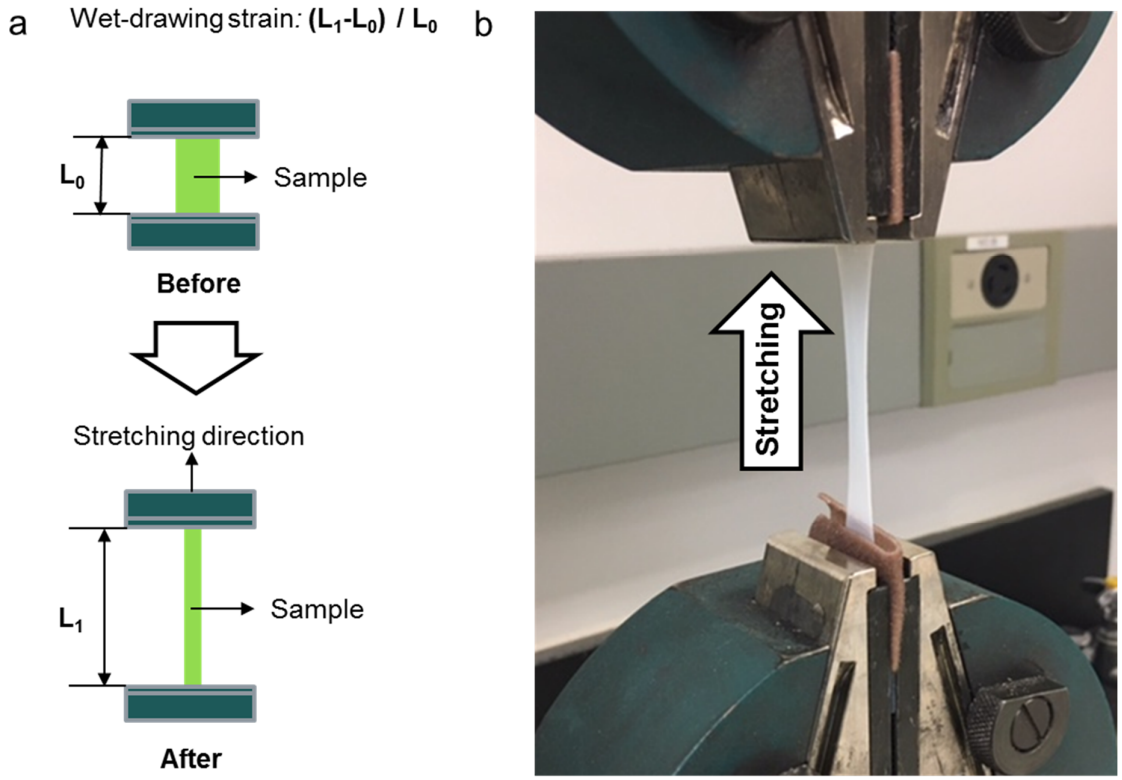

Figure S2. (a) Schematic of the stretching process and the definition of wet-drawing strain. (b) A BC pellicle is mounted between two grips, then becomes longer and narrower due to stretching caused by upward motion of the top grip.

Mechanical performance of wet BC pellilces

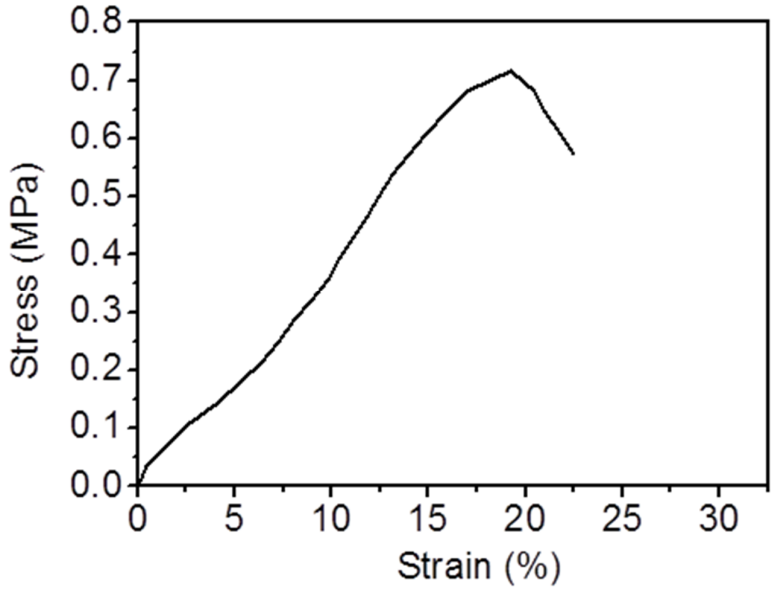

Figure S3. Stress-strain curve for wet BC pellicle. A BC pellicle with a width of 2 cm was stretched using a tensile test machine at a gauge length of 60 mm. A maximum wet-drawing strain of around 20% was observed before fracture of the cellulose nanofibrils.

SEM image of 40% stretched BC film at a low magnification.

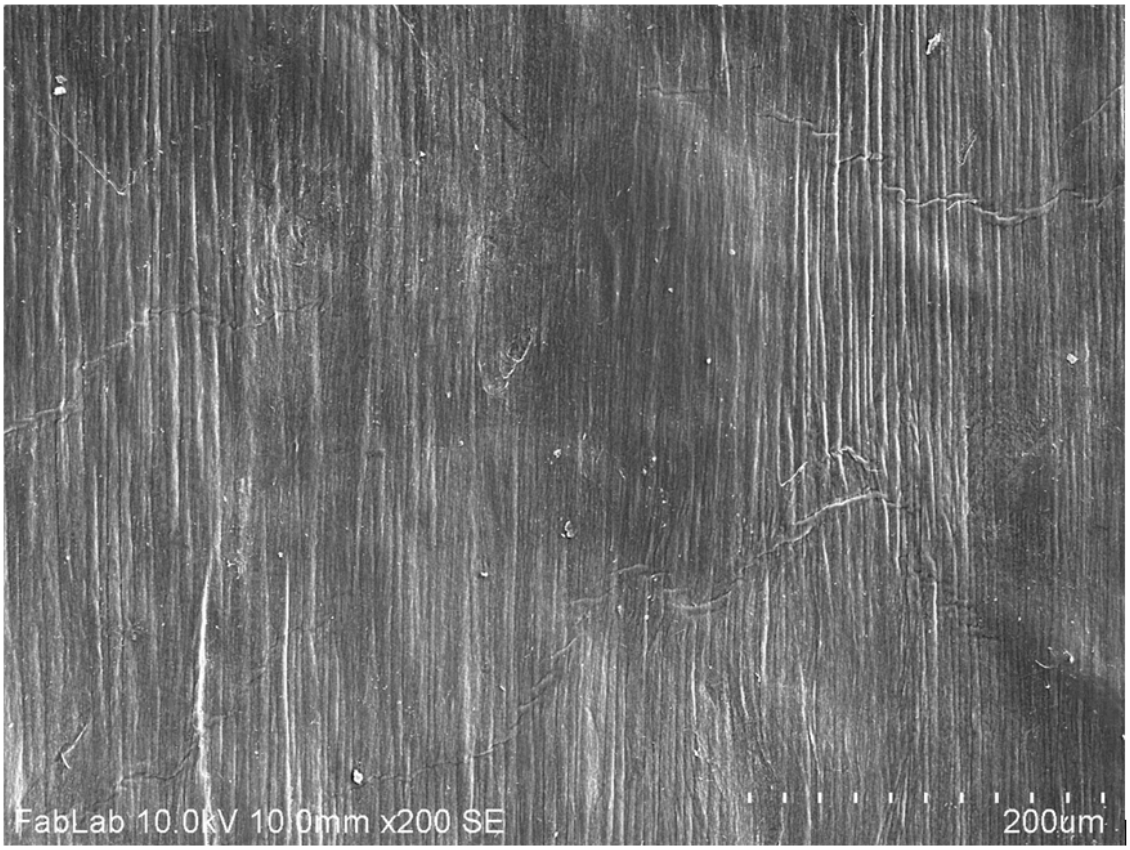

Figure S4. FE–SEM image of the surface of the 40% stretched BC film exhibiting an aligned pattern. The BC film is made from cutting and stretching the purified BC pellicle shown in Figure S1.

AFM images of BC films before and after alignment.

The surface morphologies of the resulting BC films under different wet-drawing strain levels are further analyzed by AFM (Figure S5). The as-grown BC film (0% in Figure S5) shows an isotropic structure, which is composed of randomly distributed nanofibrils. As for the 20% stretched sample, an increased degree of nanofibril orientation can be observed. Upon further increasing the drawing level, a well-aligned structure is clearly observed (30%, and 40% in Figure S5). As can be seen, the 40% stretched sample clearly shows a preferential orientation of the highly-aligned nanofibrils in the drawing direction.

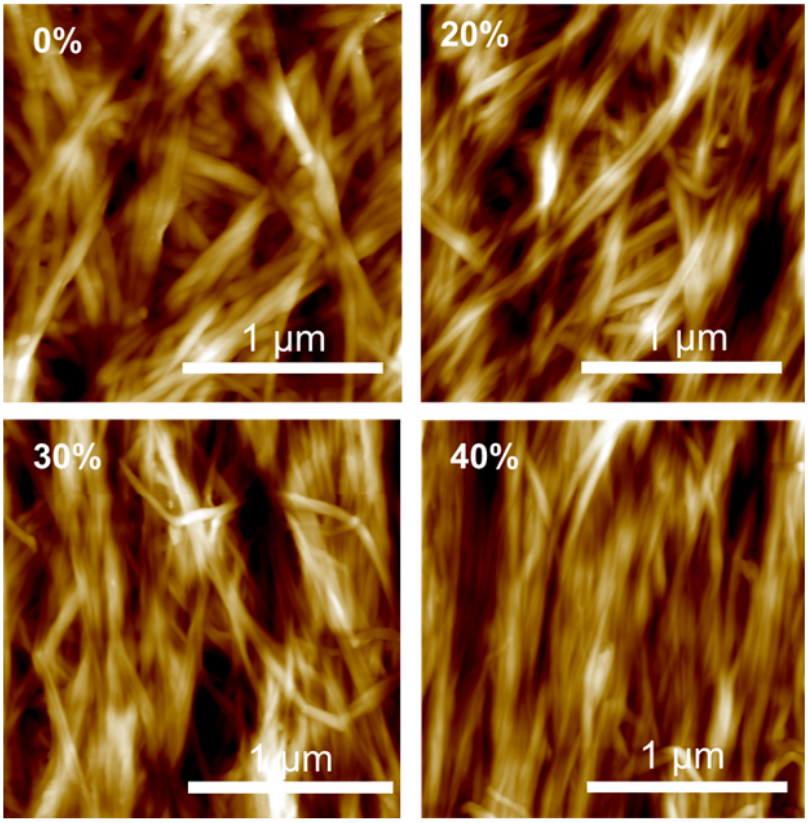

Figure S5. Typical AFM height images of BC films surfaces under 0%, 20%, 30%, and 40% wet-drawing strain, respectively, illustrating the increasing alignment with higher wet-drawing strain.

SAXS 2D patterns of BC films before and after alignment.

The original BC film shows a ring diffraction pattern, demonstrating a random structure. Upon increasing wet-drawing strain, the 2D diffraction patterns are deformed more and more, suggesting an alignment at the microscopic level, which is consistent with the previous SEM results.

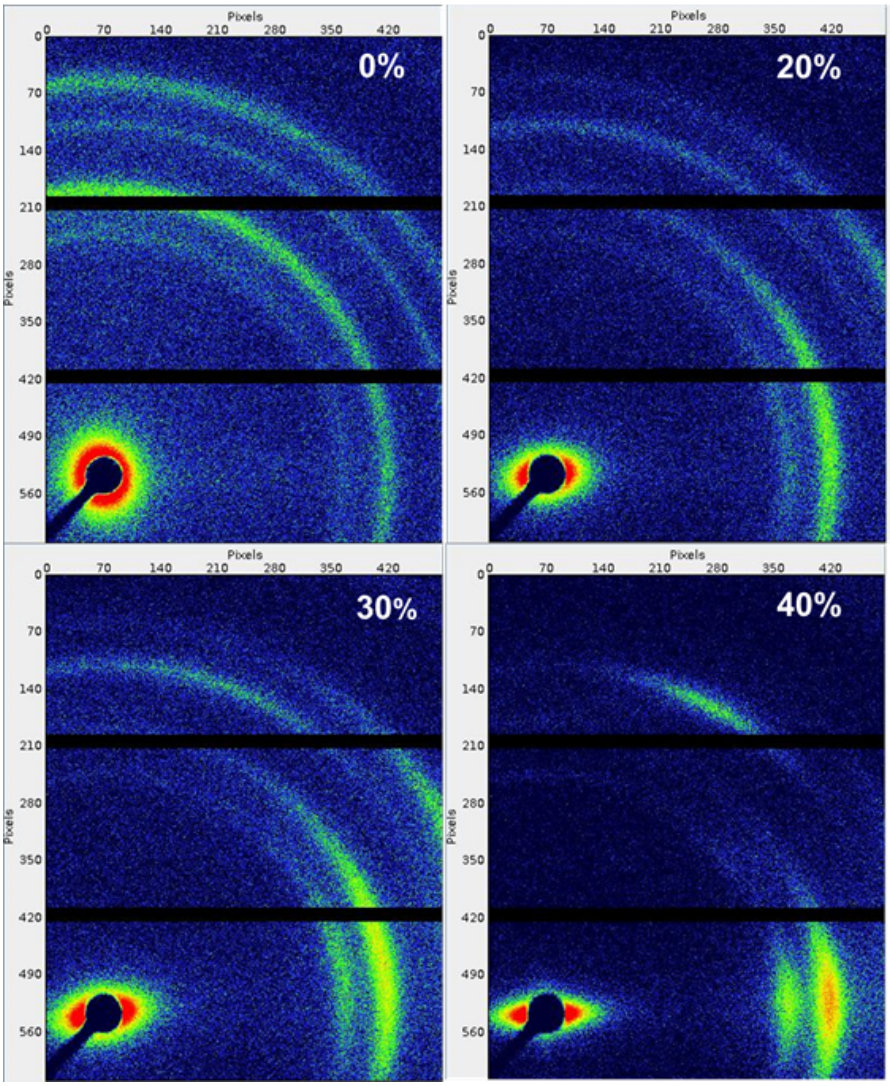

Figure S6. SAXS images of BC films before and after alignment. Typical SAXS patterns obtained for BC films under 0%, 20%, 30%, and 40% wet-drawing strain. The gradual deformation of 2D patterns (from 0% to 40%) indicates a clear trend of increasing alignment.

Fracture surface of aligned BC film

Figure S7 shows the morphology of BC fibers on the fracture surface of 40% wet-drawing BC film after stretching test. BC nanofibrils bundles are well parallel to each other due to the alignment process. The inset shows a photograph of the aligned BC film after a stretching test. The yellow box indicates the observation site under the optical microscope.

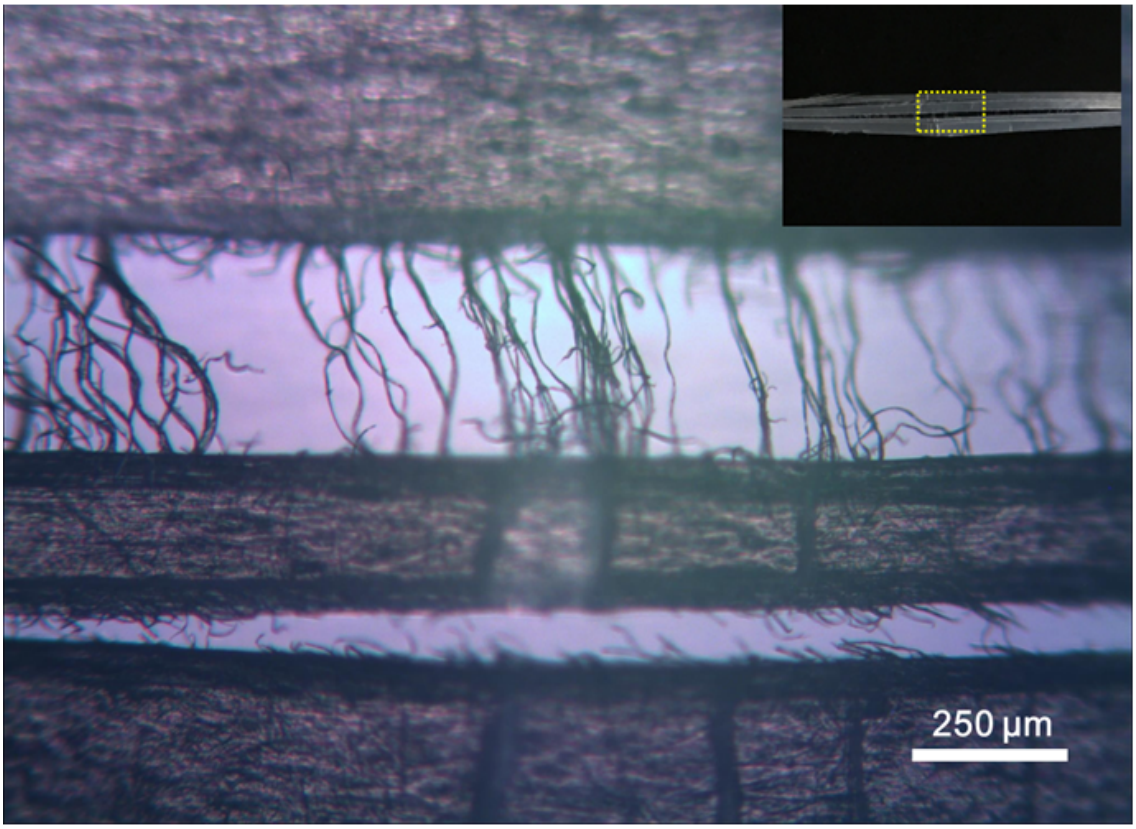

Figure S7. Morphology of fracture surface of aligned BC film at 40% wet-drawing strain. An optical microscope image of an aligned BC after a stretching test, clearly showing that the strongly aligned BC fibers are parallel to each other.

Table S1. Comprehensive comparisons of our developed BC film with some typical previously reported BC films and other cellulose films.

Sample Name	**Fabrication Method**	**Microstructure**	**Mechanical properties (strength, toughness)**		**Fundamental insight (yes or no)**	**Refs**
Highly aligned BC film	**Well-developed stretching (stretching-shaking)**	**Well-aligned, compact**	**~1GPa**	**24.7 MJ m^{-3}**	**Yes**	**This work**
Oriented nanofibrous BC film	Stretching	Partially aligned	179 MPa	0.009 MJ m^{-3}	No	Ref. 1
Stretched BC arrays	Guided BC growth and wet-stretching	Partially aligned	260 MPa	3.5 MJ m^{-3}	No	Ref. 2
PEG grafted CNF ribbon	Stretching	Aligned	576 MPa	10.9 MJ m^{-3}	No	Ref. 3
NFC film	Axially drawing	Aligned	474 MPa	4.9 MJ m^{-3}	No	Ref. 4
NFC nanopaper	Cold drawing	Poor alignment	428 MPa	6.56 MJ m^{-3}	No	Ref. 5

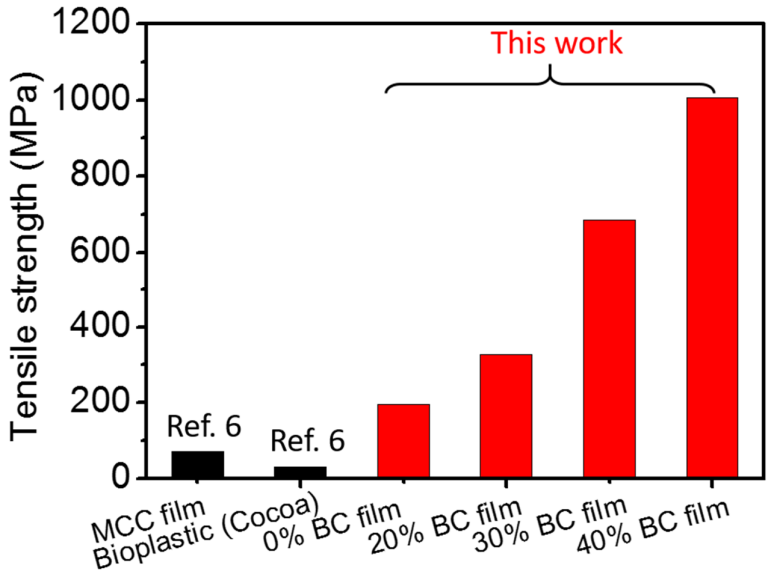

Figure S8. Mechanical properties comparison of BC films in our work with other cellulose films.

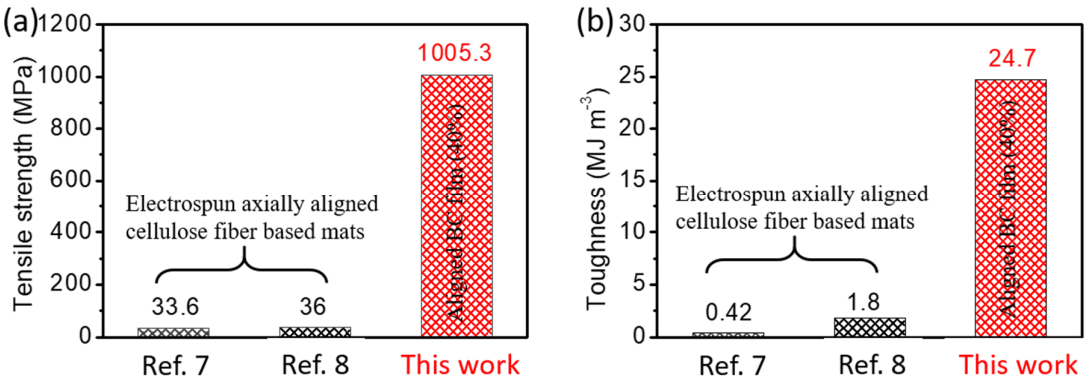

Figure S9. Mechanical properties comparison between the electrospun aligned cellulose nanofiber mats and our 40% BC film: (a) Tensile strength, (b) toughness.

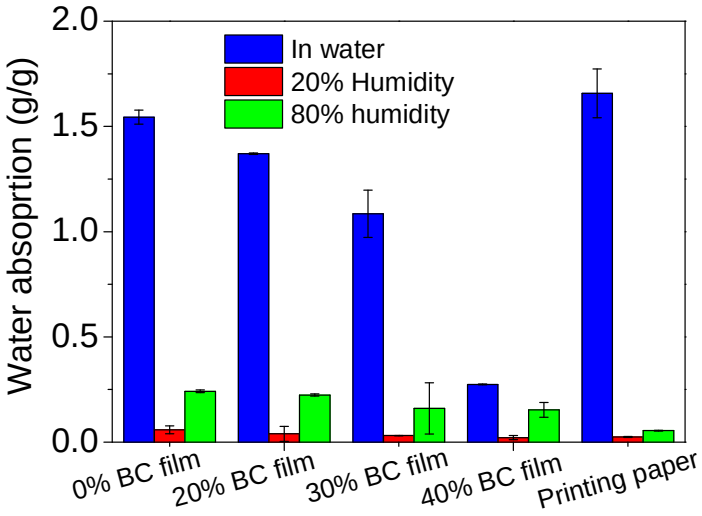

Figure S10. Water uptake of our BC films and the conventional printing paper under various humidity conditions.

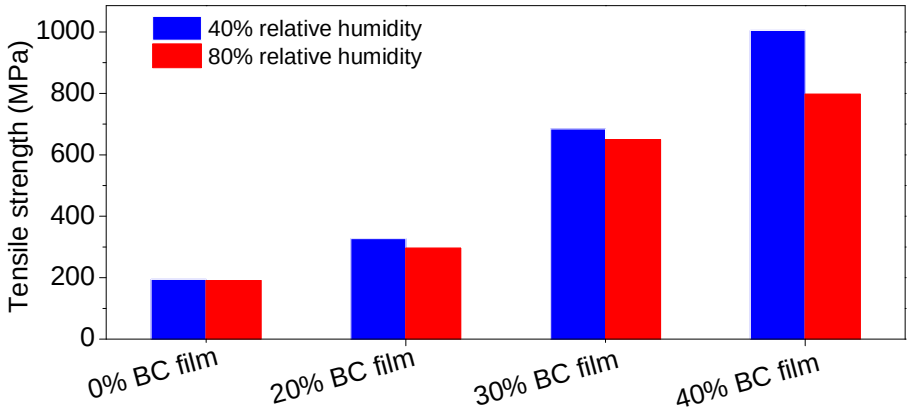

Figure S11. Humidity influence on the mechanical properties of our BC films.

Molecular dynamics simulation

The fully atomistic simulations used the ReaxFF potential[9] as implemented in the LAMMPS (Large-scale Atomic/Molecular Massively Parallel Simulator)[10] simulation package. The time step is 0.5 fs.

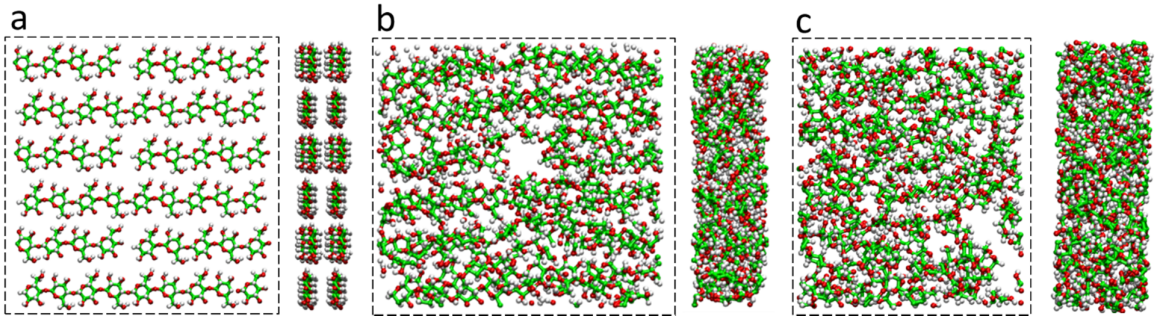

Figure S12. (a) Initial well-aligned model, for top view and side view. There are in total 12 cellulose chains (each has nine hexagonal rings) in a periodical simulation box (dashed line). Three alternating rows of cellulose chains are horizontally displaced about half the simulation box length. Green: carbon. Gray: hydrogen. Red: Oxygen. (b) Pressure-equilibrated well-aligned model. (c) Pressure-equilibrated random model.

The construction of the well-aligned model is shown in Figure S12 (a). For equilibration, the system is subjected to NPT-ensemble dynamics at a pressure of 1 atmosphere (normal pressure controlled independently) and at a temperature of 300K, using the Nosé-Hoover thermostat. The total duration of the run is 200,000 time steps. Figure S12 (b) shows the pressure-equilibrated structure. Then the mechanical deformation is applied by uniformly deforming the simulation box at a constant engineering strain rate of 0.0000025/fs, while the system is subjected to NVT ensemble with the temperature unchanged.

The construction of the randomly-dispersed model follows two steps: 1) construction of a very large simulation box and placement of 12 cellulose chains inside it so that initially they do not interact with each other. 2) execution of NVT simulation for a sufficiently long time for each cellulose chain to adopt its typical morphology. 3) execution of NVT simulations with gradual shrinking of the simulation box size so that the

cellulose chains start to aggregate. The target simulation box size is set to the one shown in Figure S12 (c). 4) Execution of NPT simulations to equilibrate the system. After this step, the mechanical deformation is applied in the same way as for the well-aligned model.

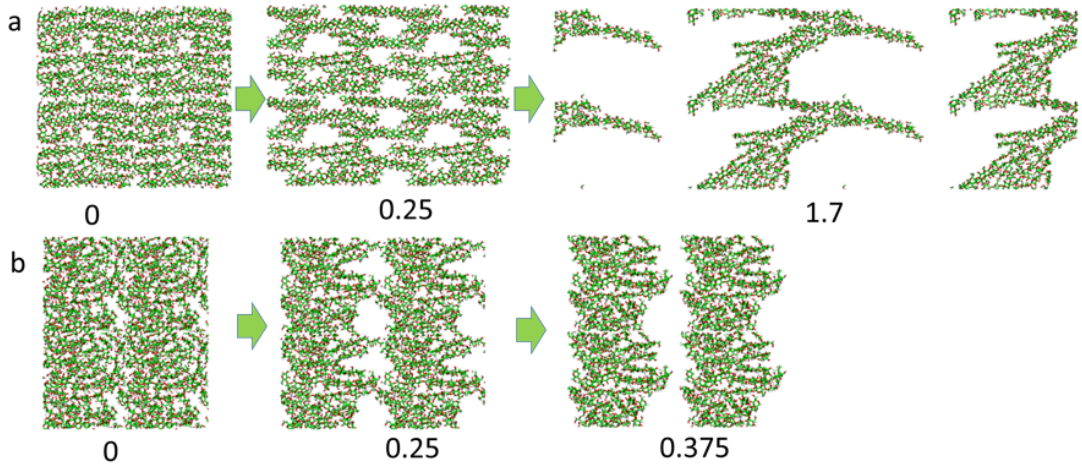

Figure S13. Deformation trajectory snapshots at different strains for the well-aligned (a), and random (b) models.

The deformation trajectory snapshots for the aligned and random models under consideration are shown in Figure S13. The virial stress is commonly used to relate to the macroscopic (continuum) stress to molecular dynamics computations.[11] At every time step during the loading, the virial stress per atom (with the units of pressure × atomic volume) is computed by the LAMMPS code. To reduce random and temperature-related stress fluctuations, we average the computed stress data every 30,000 time steps, by summing up the virial stress of every atom in the system and averaging over the occupied volume of all the atoms, which we take as the volume of the simulation box after equilibration. The loading is applied along the *x* direction and we plot the normal virial stress tensor component along the *x* direction against the engineering strain. The engineering strain is defined as the increment of the box size along the *x* direction divided by its initial length.

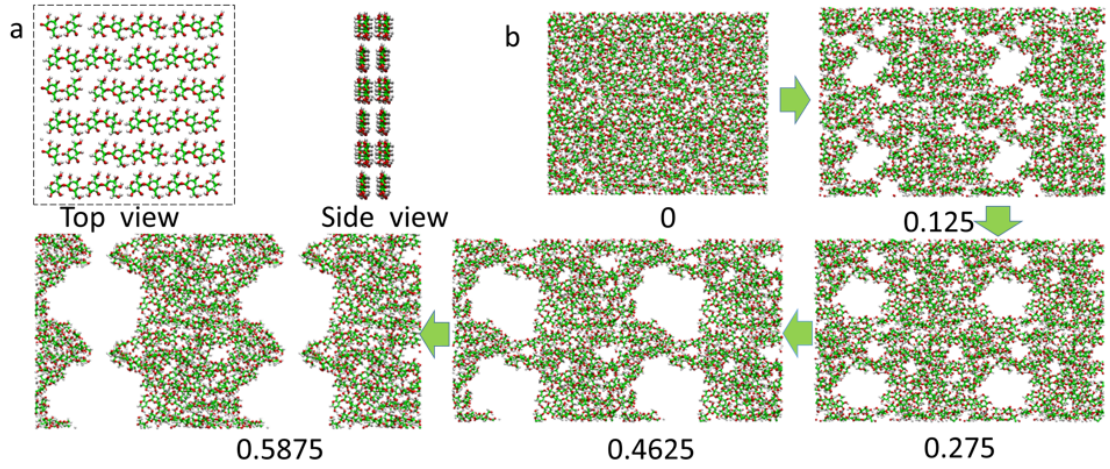

Figure S14. (a) A aligned-short model with four or five hexagonal rings (the cellulose chain is shorter than for the model shown in Figure S12 (a)). Top view and side view. (b) Deformation trajectory snapshots at different strains.

The top and side view of the aligned-short model with four or five hexagon rings is shown in Figure S14 (a). As observed from the deformation trajectory snapshots in Figure S14 (b), at a strain of 0.125, non-uniform deformation is already evident. For the model in Figure S13 (a), the deformation remains rather uniform even at a strain of 0.25. Such a difference in deformation mode causes a decrease in both maximum stress and toughness.

Light scattering setup

Figure S15 shows the light scattering setup, in which a 532 nm single mode laser (Thorlabs Inc.) was first collimated with a spot size around 200 μm before perpendicularly illuminating the samples. The incoming light rapidly diverges due to scattering within the samples.

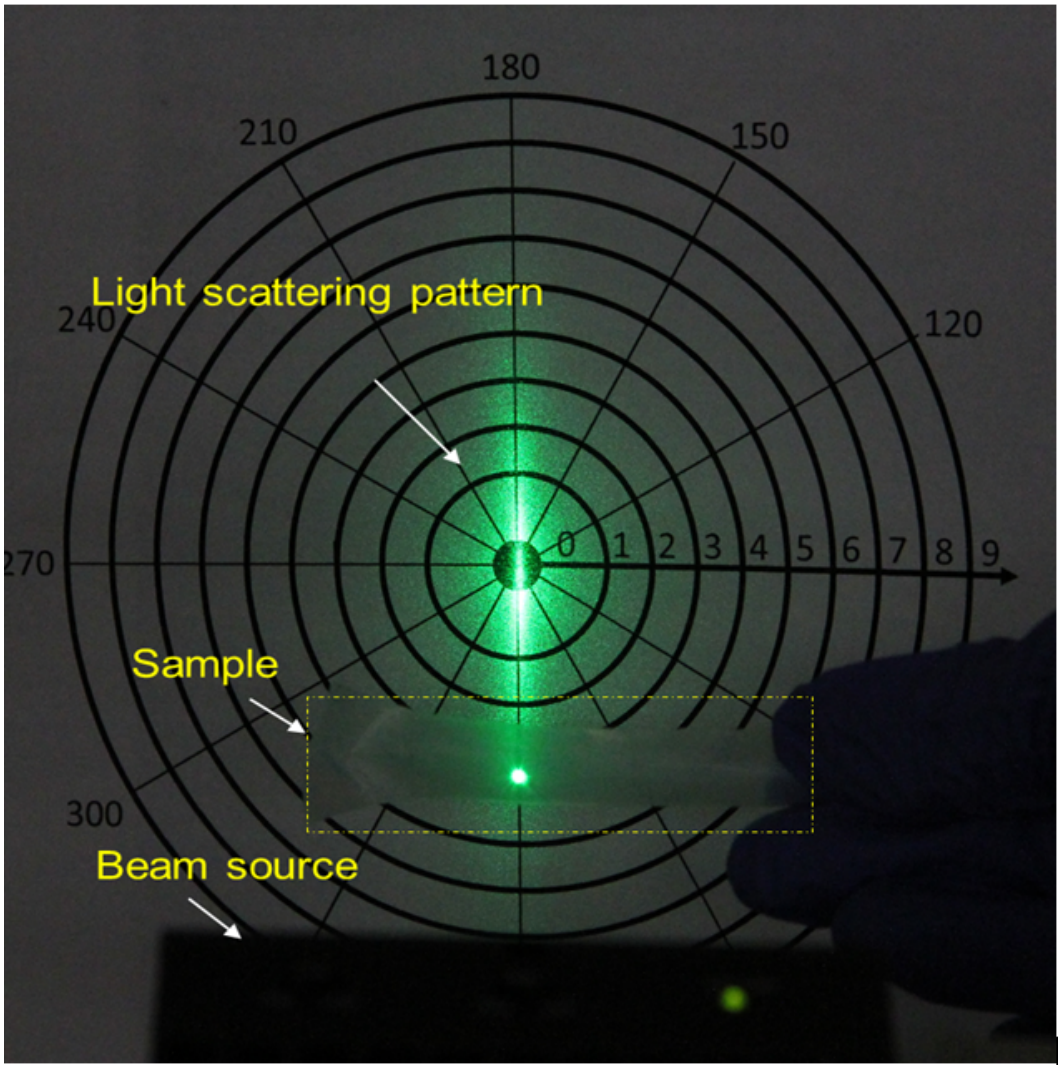

Figure S15. Light scattering setup. A green laser beam with a wavelength of 532 nm transmits through the stretched BC film and shows strong light scattering on a white screen. A 40% wet-stretched BC film is placed between a green laser beam source and a screen. Strong light scattering is observed. The yellow dashed line enclosing the sample is drawn as a visual guide.

Light scattering effects

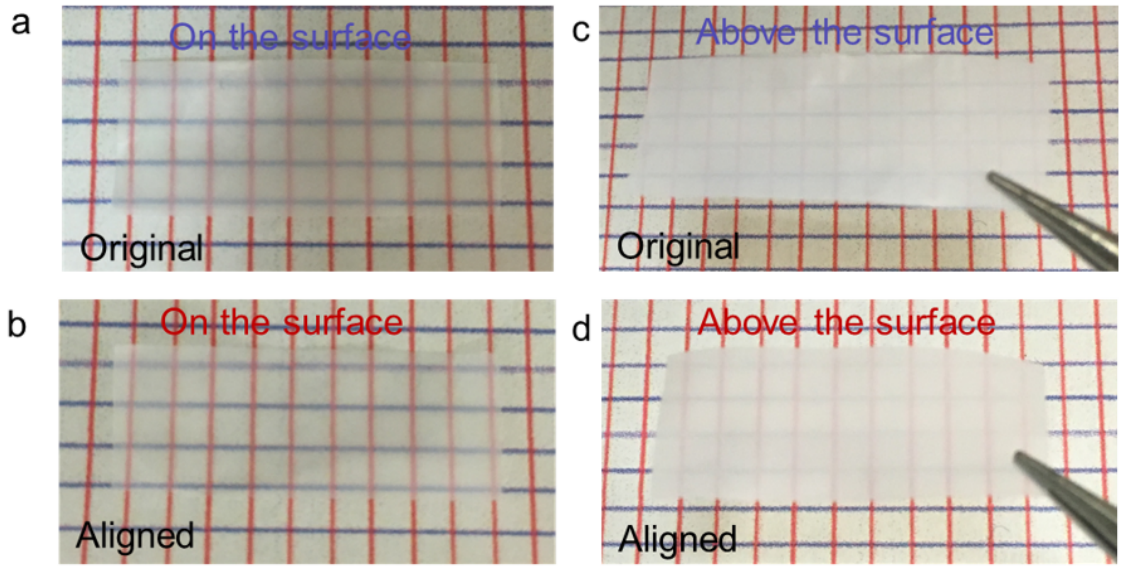

Figure S16. The original BC film is placed on (a) and above the surface (1 cm above) (b) of grids made up of parallel vertical red lines and parallel horizontal blue lines, respectively. The aligned BC film is placed on (c) and above the grid's surface (d). All lines can be clearly seen for both films when directly placing them on the surfaces of grids. For the aligned BC film, the vertical red lines are more visible than the horizontal blue lines due to anisotropic light scattering.

Figure S16 shows a unique scattering effect of the aligned BC film. Grids are made up of vertical red lines and horizontal blue lines. All lines can be clearly seen for both the original and aligned BC films when placing them directly on the surface of the grid lines (Figure S16 a, b). However, all grids lines become hazy when the original BC film is placed 1 cm above the surface due to the high transmittance haze (Figure S16 c, d). For the aligned BC film, the vertical red lines are much clearer while the horizontal blue lines appear more blurry due to anisotropic scattering effects, which are in accordance with the anisotropic haze effect shown in Figure 5a, d.

Supplementary References

[1] A. Nagashima, T. Tsuji, T. Kondo, *Carbohydr. Polym.* **2016**, *135*, 215.

[2] M. M. Rahman, A. N. Netravali, *ACS Macro. Lett.* **2016**, *5*, 1070.

[3] H. Tang, N. Butchosa, Q. Zhou, *Adv. Mater.* **2015**, *27*, 2070.

[4] C. Baez, J. Considine, R. Rowlands, *Cellulose* **2014**, *21*, 347.

[5] H. Sehaqui, N. Ezekiel Mushi, S. Morimune, M. Salajkova, T. Nishino, L. A. Berglund, *ACS Appl. Mater. Interfaces* **2012**, *4*, 1043.

[6] I. S. Bayer, S. Guzman-Puyol, J. A. Heredia-Guerrero, L. Ceseracciu, F. Pignatelli, R. Ruffilli, R. Cingolani, A. Athanassiou, *Macromolecules* **2014**, 47, 5135.

[7] X. He, Q. Xiao, C. Lu, Y. Wang, X. Zhang, J. Zhao, W. Zhang, X. Zhang, Y. Deng, *Biomacromolecules* **2014**, 15, 618.

[8] H. Q. Liao, Y. Q. Wu, M. Y. Wu, X. R. Zhan, H. Q. Liu, *Cellulose* **2012**, 19, 111.

[9] T. R. Mattsson, J. M. D. Lane, K. R. Cochrane, M. P. Desjarlais, A. P. Thompson, F. Pierce, G. S. Grest, *Phys. Rev. B* **2010**, 81, 054103.

[10] S. Plimpton, *J. Comput. Phys.* **1995**, 117, 1.

[11] D. Tsai, *J. Chem. Phys.* **1979**, 70, 1375.